









Article

Analysis of the Recharge Area of the Perrot Spring (Aosta Valley) Using a Hydrochemical and Isotopic Approach

Luis Miguel Santillán-Quiroga ^{1,2}, Daniele Cocca ^{1,*}, Manuela Lasagna ^{1,*}, Chiara Marchina ³, Enrico Destefanis ¹, Maria Gabriella Forno ¹, Marco Gattiglio ¹, Giacomo Vescovo ¹
and Domenico Antonio De Luca ¹

¹ Earth Science Department, University of Turin, Via Valperga Caluso 35, 10125 Torino, Italy; luismiguel.santillanquiroga@unito.it (L.M.S.-Q.); enrico.destefanis@unito.it (E.D.); gabriella.forno@unito.it (M.G.F.); marco.gattiglio@unito.it (M.G.); giacomo.vescovo@unito.it (G.V.); domenico.deluca@unito.it (D.A.D.L.)

² Facultad de Ciencias, Escuela Superior Politécnica de Chimborazo, Km 1 1/2 Panamericana Sur, Riobamba EC060155, Ecuador

³ Department of Land, Environment, Agriculture and Forestry, University of Padova, Viale dell'Università 16, 35020 Legnaro, Italy; chiara.marchina@unipd.it

* Correspondence: daniele.cocca@unito.it (D.C.); manuela.lasagna@unito.it (M.L.); Tel.: +39-11-670-5117 (D.C.); Tel.: +39-32-8415-5324 (M.L.)

Abstract: The Perrot Spring (1300 m a.s.l.), located to the right of the Chalamy valley in the Monte Avic Natural Park (Valle d'Aosta, Italy), is an important source of drinking water for the municipality of Champdepraz. This spring is located on a large slope characterised by the presence of a Quaternary cover of various origins (glacial, glaciolacustrine, and landslide) above the bedrock (essentially serpentinite referred to the Zermatt–Saas Zone, Penninic Domain). Water emerges at the contact between the landslide bodies and impermeable or semi-permeable glaciolacustrine deposits. The aim of this study is to define the processes and recharge zones of this spring. The analysis of the data revealed the presence of two contributions to the Perrot Spring input: a spring thaw contribution defined by a small increase in flow and an autumn contribution from rainwater infiltration. The low average temperature and low variation of the annual temperature (4.8–6.5 °C) suggest a sufficiently deep flow circuit. Chemical analyses showed a groundwater chemistry consistent with the regional geology: the hydrochemical facies is calcium–magnesium bicarbonate and isotopic analyses ($\delta^2\text{H}$ and $\delta^{18}\text{O}$) of rainfall and spring water suggested a recharge altitude of about 2100 m a.s.l. In conclusion, this study makes it possible to recognize the water inputs to the spring discharge and to delineate its recharge area, which can be proposed to implement strategies to protect the resource.

Keywords: spring; recharge area; Alps; Mont Avic Natural Park; water stable isotopes; hydrochemistry



Citation: Santillán-Quiroga, L.M.; Cocca, D.; Lasagna, M.; Marchina, C.; Destefanis, E.; Forno, M.G.; Gattiglio, M.; Vescovo, G.; De Luca, D.A. Analysis of the Recharge Area of the Perrot Spring (Aosta Valley) Using a Hydrochemical and Isotopic Approach. *Water* **2023**, *15*, 3756. <https://doi.org/10.3390/w15213756>

Academic Editors: José Manuel Marques and Paula M. Carreira

Received: 28 September 2023

Revised: 23 October 2023

Accepted: 25 October 2023

Published: 27 October 2023



Copyright: © 2023 by the authors. Licensee MDPI, Basel, Switzerland. This article is an open access article distributed under the terms and conditions of the Creative Commons Attribution (CC BY) license (<https://creativecommons.org/licenses/by/4.0/>).

1. Introduction

Water is an essential resource that will become increasingly important over time as population and crop water needs grow, rendering the planning and maintenance of sustainable drinking water resources a major challenge for human societies [1,2]. Given its importance as a drinking water resource, there is an increasing need to understand recharge patterns and to monitor the effects of changing climatic conditions on water reserves.

Mountain springs are one of the most strategic water resources in some parts of Italy [3–5]. In a typical high mountain environment, aquifers feed springs along the slopes [6]. The research on the springs includes the characterization of parameters such as air temperature and rainfall at different time and event scales [7,8]. This analysis, together with electrolytic conductivity, gives an indication of the type of spring [9]. In this

context, it is essential to preserve the recharge zone [10], which plays an important role in management, conservation, and restoration over time [11].

Estimating aquifer recharge is key to effective groundwater management and protection. In mountain areas, average annual spring discharge generally reflects the aquifer recharge across the spring catchment [12]. While the carbonate reliefs represent large recharge zones, mainly feeding regional aquifers due to fracturing and karst processes, in other contexts, such as the one studied, the recharge area is smaller, and the role of unconsolidated deposits and fractured bedrock is important. In the western Alps, for example, the Montellina spring is recharged by highly fractured bedrock thanks to a wide and thick glacial sediment cover and buried glacial valleys [13,14].

Hydrogeochemical methods have been widely used to understand recharge processes. Hydrochemical and isotopic data can be used to reconstruct the flow paths and storage characteristics of springs [15,16]. Indeed, water–rock interactions result in a kind of natural dynamic fluid under the control of the environment and rock structure [17].

Stable isotopes of water have been used for decades as tracers of the global water cycle [18–21]. Several studies using the stable isotopes of water ($\delta^2\text{H}$ and $\delta^{18}\text{O}$) have shown that water recharge processes depend on (i) climate conditions, (ii) geological/topographic conditions, (iii) land cover and soil properties, and (iv) seasonal variations [22,23]. The hydrological system of the Aosta Valley is complex, linked to the circulation of humid air masses, to the relative orientation and geographical position of the valleys in relation to these circulations, and to the role of the glaciers and their associated rocky substratum in modifying the quality and quantity of their runoff [24]. Some authors [25], using stable isotopes of water, showed, for example, a predominant influence of Mediterranean air masses on the karst aquifer near the Slovenian–Italian border. They also observed how some types of water are influenced by water–rock interaction processes and meteoric water infiltrating at depth from the Triassic evaporite belonging to the Tuscan sedimentary series forming the surrounding reliefs (central Italy) [26]. In addition, stable isotopes of water have been used as inert tracers to indicate the residence time of groundwater in aquifer systems and potential sources of recharge [27–30].

In the last decade, the demand for accurate spatio-temporal predictions of $\delta^2\text{H}$ and $\delta^{18}\text{O}$ values of rainfall at point, regional, and continental scales has increased [31], including the application of high-resolution in situ sampling of stable isotopes in the unsaturated zone, stream water, and rainfall [32,33], particularly by increasing and improving the amount of information in areas where few or no data exist, such as the tropics [34,35]. For example, stable isotopes of water have identified different altitudes for the recharge zone of the Chiche and Ilaló aquifers in Ecuador [36]. Similarly, [37] showed that the $\delta^2\text{H}$ and $\delta^{18}\text{O}$ stable isotope technique can be applied to hydrological models from local and regional to meso-global scales in China. Even rainfall dominated by inland moisture from continents has been revealed using stable isotopes of water and d-excess values of stream water in a mountain basin around the Qinghai–Tibet Plateau [38]. Away from coastal influences, surface water and groundwater are derived exclusively from rainfall [39]. These isotopic methods are so important in combination with hydroclimatic records [22] that they help us to understand the season of the year of maximum aquifer recharge [39], and the differences between the slopes and intercepts in the correlation graphs between $\delta^2\text{H}$ and $\delta^{18}\text{O}$ when different regression methods are used, regardless of the type of water studied; for example, the stronger the correlation between $\delta^2\text{H}$ and $\delta^{18}\text{O}$ in the dataset, the smaller the difference between their slopes [40].

The Perrot Spring, located in the Mont Avic Natural Park (Aosta Valley, Italy), is an important source of drinking water for the community of Champdepraz. However, this spring has been poorly studied in the past. The aim of our study is to increase our knowledge on the recharge of the Perrot Spring, as a significant example that can help to improve the protection of water resources in mountain areas and, above all, to ensure sustainable management in the long term.

2. Study Area Description

2.1. Study Area

The study area is located in Northwestern Italy and is entirely within the territory of the Aosta Valley (Figure 1).

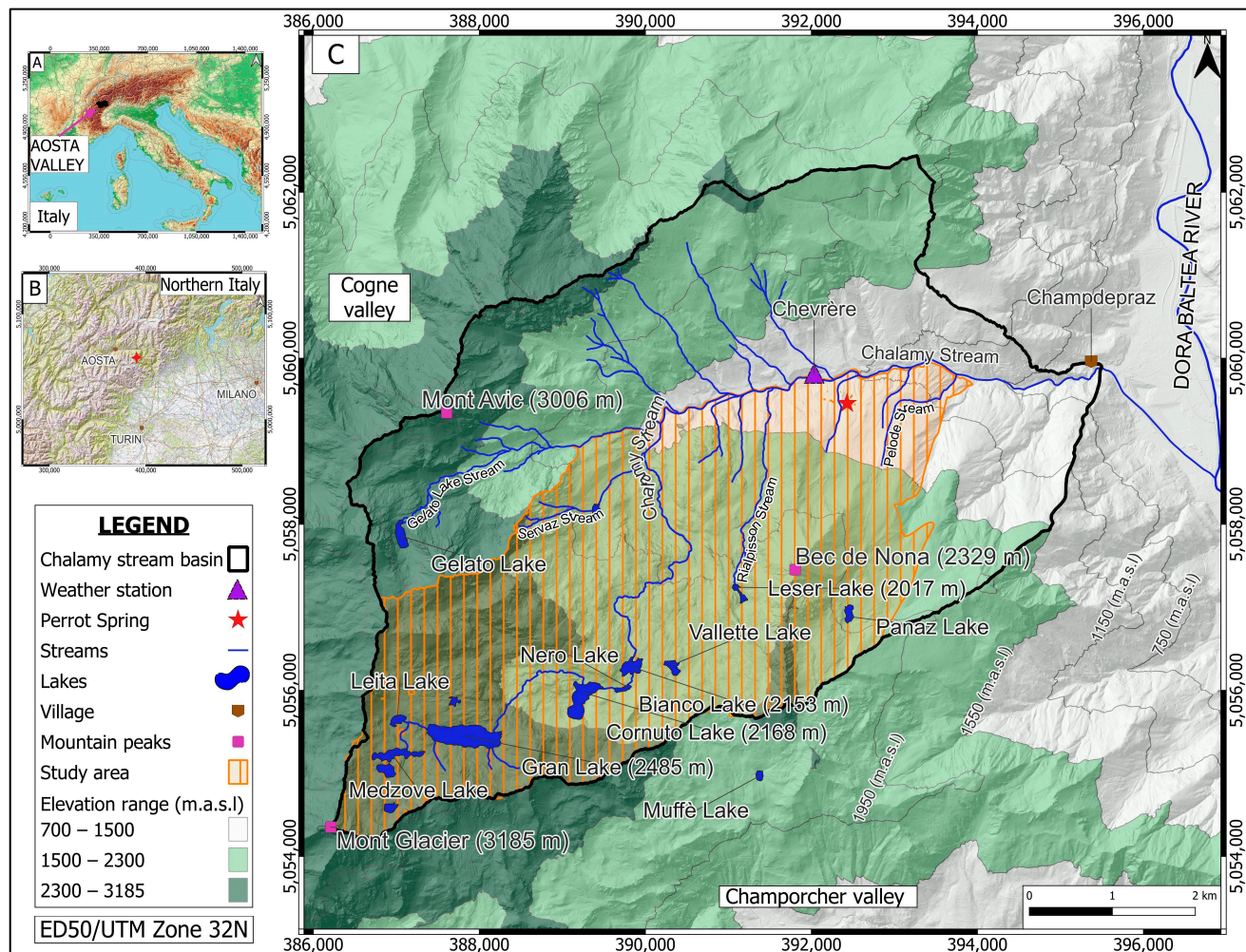


Figure 1. (A) Location of Aosta Valley in Italy. (B) Location of the study area (asterisk) in Northwestern Italy. (C) Location of the investigated area in the Chalamy Basin.

The Perrot Spring, studied in this research, is located in the central-eastern part of the Aosta Valley, in the municipality of Champdepraz. More specifically, the spring is in the Chalamy Valley at an altitude of 1300 m above sea level (a.s.l.), on the right orographic slope (Figure 1). Altimetrically, the investigated area is located between 3185 m a.s.l. of Mont Glacier and 850 m a.s.l. of the Chalamy Valley floor, that covers a surface of approximately 28 km².

2.2. Geological Setting

The study area is located in the Penninic Domain [41] and, more specifically, within the Piedmont Zone. This zone has been affected by alpine peak metamorphism in HP–LT conditions (eclogite and blue schist facies) with subsequent re-equilibration in green schist facies metamorphism and is characterised by the presence of serpentinite with minor masses of prasinite, amphibolite, talcoschist, calcareous schist, and prasinic gneiss [41–47].

More specifically, the investigated area lies within the Mont Avic Massif which represents one of the ophiolite massifs in the Western Alps [48–50] (Figure 2). This massif essentially consists of serpentinitised peridotite with ochre- to reddish-brown-coloured

weathered surface and dark green to black fresh surface. Serpentinite is mainly composed of serpentine (0.1–1 mm-sized antigorite crystals) and magnetite (up to mm-sized) which defines the main foliation. Abundant intercalations of magnetite chloritoschist and rodingitic bodies also occur. Associated with the ultra-basic rocks are a few eclogitic metagabbro bodies and metabasalt. Rare metasedimentary pelagic cover is mostly represented by quartzite and saccharoid marble. This ophiolitic sequence, which underwent peak metamorphism in eclogitic facies during alpine metamorphism, is tectonically covered by the Glacier-Refray Austroalpine klippe [43,51]. This klippe, outcropping in the western border of the study area, is mainly composed of albitic minute gneiss and garnet micaschist.

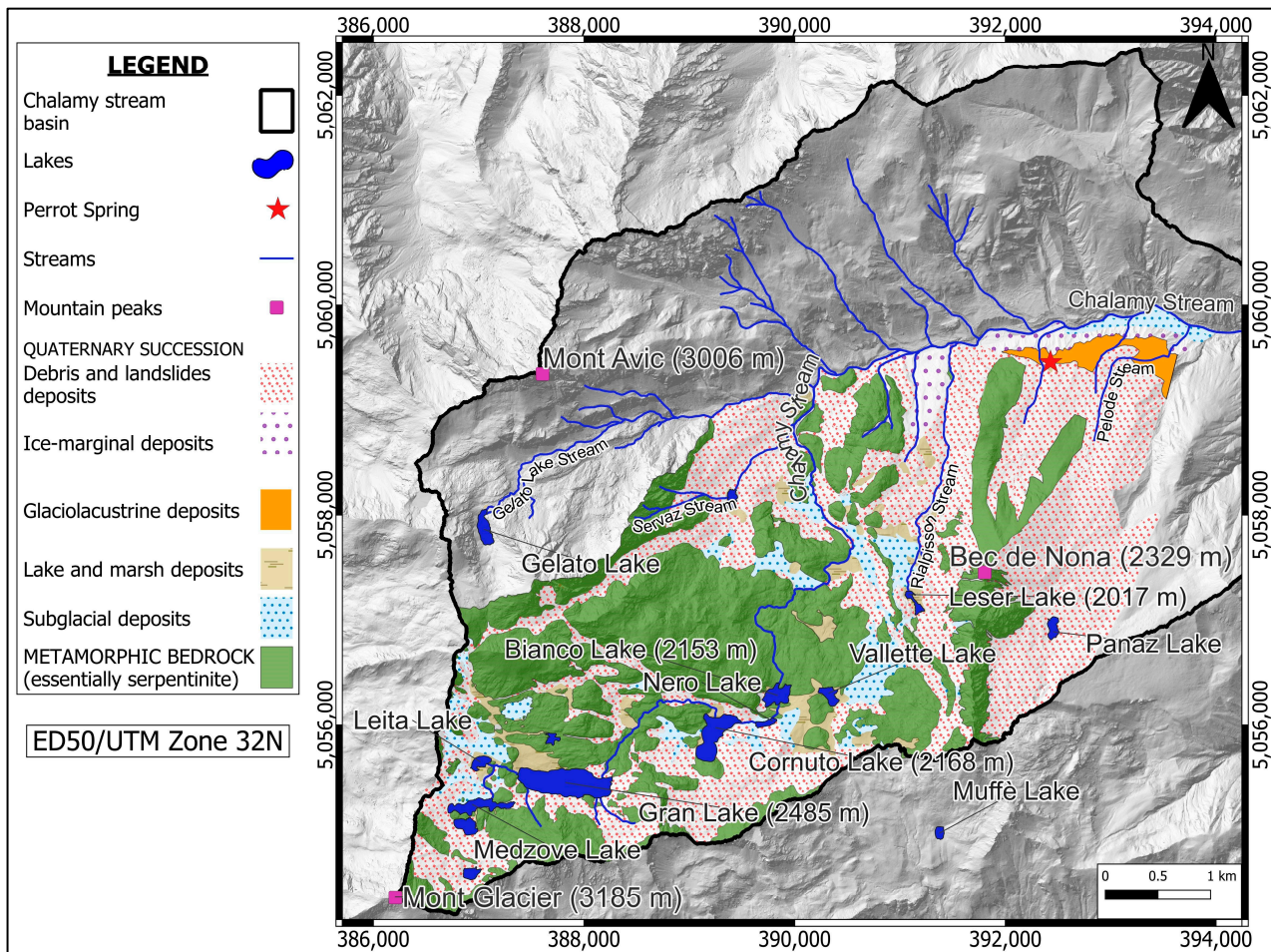


Figure 2. Geological map of the study area.

Quaternary unconsolidated, very thick (up to 240 m) sediments diffusely cover the metamorphic bedrock on the wide valley floor, where they crop out in large badlands. They consist of overlapped subglacial, ice-marginal, glaciolacustrine and landslide deposits [52] (Figure 2). The subglacial over consolidated sediments (30 m thick) consist of abundant sandy–silty matrix, containing subordinate clasts, that were deposited at the base of the Chalamy Glacier.

The ice-marginal deposits (from 100 to 150 m thick) consist instead of clasts of very different sizes mixed in a subordinate matrix and rich in very large boulders (up to 1000 m³). These sediments, that were deposited at the edges of the Chalamy Glacier and formed two lateral moraines preserved on the two sides of the valley, show a bedding towards the external edges of the moraines.

Glaciolacustrine sediments (100 m thick) are formed by alternating fine- and coarse-grained sediments, which form a wide glaciolacustrine terrace. The most abundant fine sediments are characterized by planar-parallel bedding (with dips towards the SSE) and

show a sandy-silty matrix in which some centimetric to decimetric clasts occur. These alternating fine- and coarse-grained sediments are typical of lakes formed at the edge of the Dora Baltea Glacier at the confluence of the tributary valleys [53].

The landslide sediments, forming a convex fan which is several tens of metres thick, are coarse-grained and consist of prevalent clasts of various sizes mixed in a subordinate sandy-silty matrix. The succession of various types of Quaternary sediments greatly influences the genesis of the Perrot Spring, as suggested by the location of this spring at the interface between the glaciolacustrine and the landslide sediments.

2.3. Hydrogeological Setting

The different rocks of the study area (metamorphic bedrock and Quaternary cover) were grouped according to their geological and hydrogeological characteristics in different hydrogeological units (Figure 3):

1. Metamorphic bedrock.

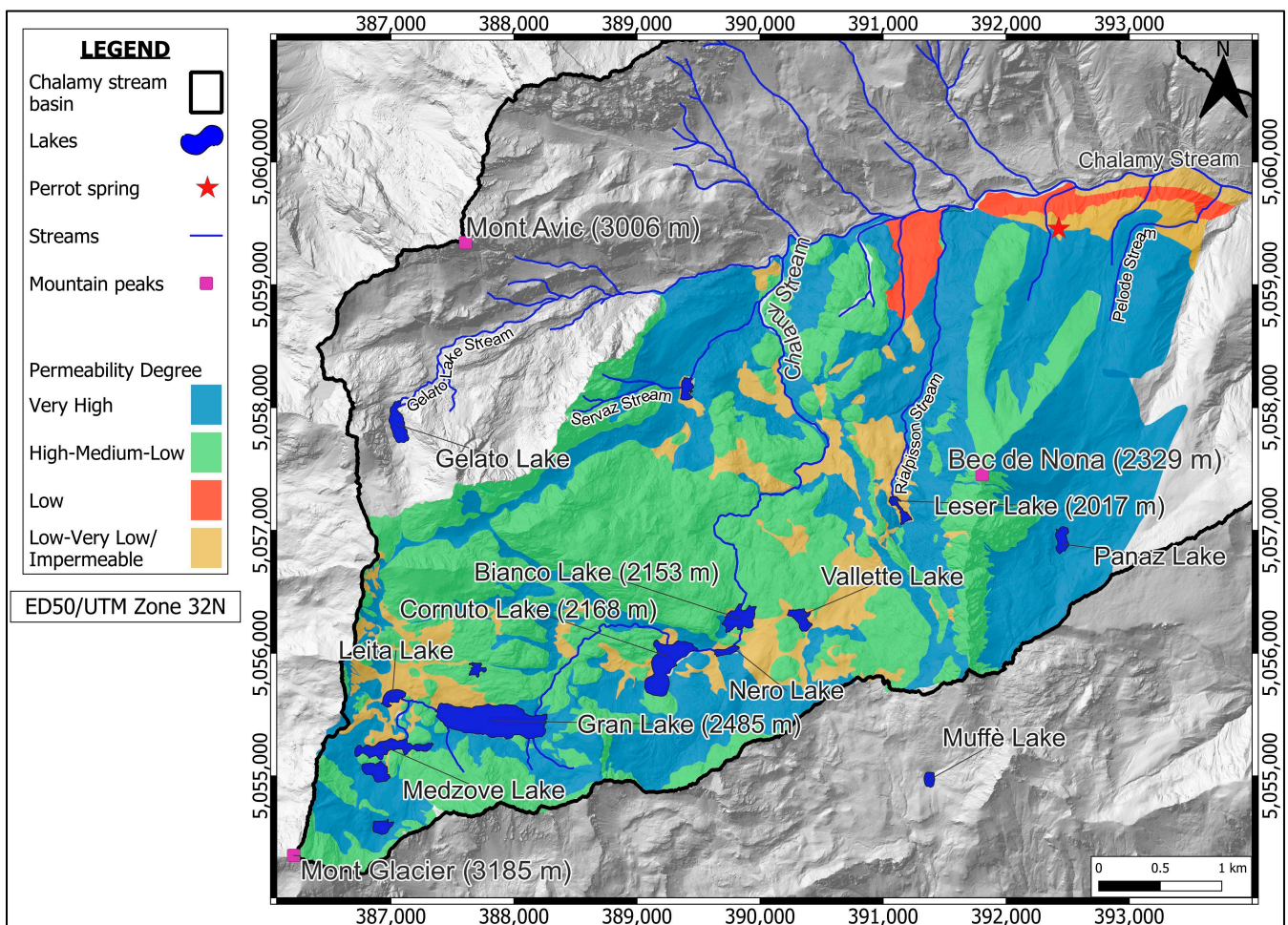


Figure 3. Map of permeability degree.

This is variously fractured essentially peridotite with predominantly massive structure and local presence of foliated portions rocks, deformed on small and medium scales. Permeability is dependent on the degree of fracturing.

2. Quaternary succession.

- Subglacial deposits: over consolidated deposits characterized by abundant sandy-silty matrix containing subordinate clasts. Low permeability;

- Ice-marginal deposits: deposits with a very heterogeneous texture, characterised by the presence of clasts of different sizes and shapes, mixed in a greyish-brown sandy–silty matrix with carbonate cementation. Variable permeability;
- Glaciolacustrine deposits: deposits formed by a sandy–silty matrix in which some centimetric to decimetric clasts are embedded, showing carbonate cementation. Low permeability;
- Debris and landslide deposits: deposits formed by angular decimetric clasts without matrix. Very high permeability;
- Lake and marsh deposits: silty and peat deposits characterised by a very localised distribution in depressed areas. Low permeability.

In Table 1, rocks of the study area were schematized based on the hydrogeological characteristics (degree and type of permeability).

Table 1. Hydrogeological units in the study area.

Lithology		Hydraulic Conductivity k (m/s)	Type of Permeability
Lake and marsh deposits		Very low ($10^{-7} > k > 10^{-9}$)	Porosity
Debris and landslide deposits		Very high ($k > 10^{-2}$)	Porosity
Subglacial deposits		Very low ($10^{-7} > k > 10^{-9}$)	Porosity
Ice-marginal deposits		Low ($10^{-5} > k > 10^{-7}$)	Porosity
Glaciolacustrine		Low and very low ($10^{-5} > k > 10^{-9}$)	Porosity
Metamorphic bedrock (serpentinite)	Fractured	Low ($10^{-5} > k > 10^{-7}$)	Fractures
	Mylonitized	Medium ($10^{-4} > k > 10^{-5}$)	
	Foliate and fractured	High ($10^{-2} > k > 10^{-4}$)	
	Massive	Impermeable ($k < 10^{-9}$)	

3. Materials and Methods

3.1. Climatic Conditions

In order to better understand the climatic characteristics of the study area, a weather station (Chevrère Station), belonging to the Autonomous Region of Valle d’Aosta, was utilized [54]. This station, located at 1260 m a.s.l. in the Chalamy stream basin (Figure 1), is the closest to the Perrot Spring. Specifically, air temperature and rainfall data, downloaded from [54], were collected with a daily frequency. The data were aggregated into monthly and annual average data for the period 2003–2022.

3.2. Water Sampling

Six sampling campaigns were conducted in May, July, and November 2021, and in February, July, and September 2022. The 19 sampling points included water from the Perrot Spring ($n = 1$), rainfall ($n = 6$), lakes ($n = 10$), and streams ($n = 2$) within the Chalamy Basin (Figure 4) (Table 2). In the field, temperature, electrolytic conductivity (EC), and pH were measured with a Hanna HI98130 m and then repeated in the laboratory (resolution, precision of temperature samples 0.1 °C, 0.5 °C; EC: 0.01 mS/cm, 2% full scale; pH: 0.01, 0.05). At each sampling point, two samples were collected in polyethylene bottles (250–500 mL) for chemical and isotopic analysis. The location of the rainwater collectors was chosen to conduct an isotopic study and, more specifically, to determine the isotope gradient (Figure 4). The rain samplers were HDPE containers connected to a funnel which acted as a rainfall conveyor inside the container. A layer of paraffin oil (0.5 cm) was inserted in the container to prevent or significantly reduce the loss of water by evaporation. A fine-mesh net was attached to the top of the funnel and used as a filter for any material that may obstruct the rainwater inlet during the sampling period.

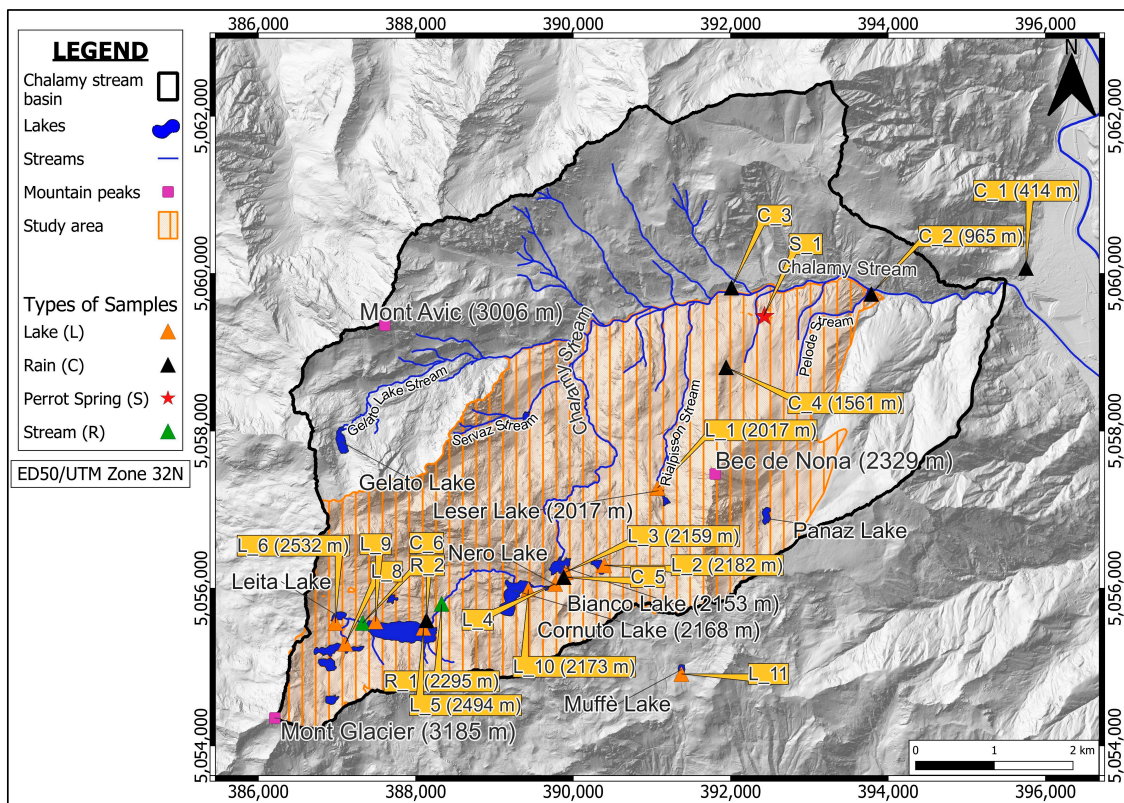


Figure 4. Water sampling points in the study area: rainfall collectors, streams, lakes, and the Perrot Spring. See Table 2 for co-ordinates.

Table 2. Water sampling points (C: rain, S: Perrot Spring, R: stream, and L: lake). (A: Isotopic analyses; B: Chemical analyses).

Monitoring Point ID	Location	X UTM ED 50	Y UTM ED 50	Elevation (m a.s.l.)	2021				2022		
					1 May	6 May	3 July	11 November	7 July	8 July	20 September
C_1	Park Office	395,752	5,060,071	414	x			x		x	
C_2	Park Location 2	393,786	5,059,742	965	x			x		x	
C_3	Park Location 3	392,011	5,059,822	1269	x			x		x	
C_4	near Perrot Spring	391,942	5,058,810	1561				x		x	
C_5	near Bianco Lake	389,798	5,056,012	2160					x		x
C_6	near Gran Lake	388,078	5,055,339	2503							x
S_1	Perrot Spring	392,417	5,059,457	1300	x	x			x	x	x
R_1	Chalamy Stream	388,314	5,055,804	2295						x	x
R_2	Chalamy Strea	387,318	5,055,539	2532						x	x
L_1	Leser Lake	390,992	5,057,071	2017						x	x
L_2	Vallette Lake	390,305	5,056,100	2182						x	x
L_3	Bianco Lake	389,818	5,056,055	2159			x			x	x
L_4	Nero Lake	389,718	5,055,861	2169			x			x	x
L_5	Gran Lake	388,055	5,055,272	2494			x			x	x
L_6	Leita Lake	386,974	5,055,430	2532						x	x
L_8	Leita Superiore Lake	387,008	5,055,058	2563						x	x
L_9	North of the Gran Lake	387,567	5,055,658	2527						x	x
L_10	Cornuto Lake	389,378	5,055,834	2173			x			x	x
L_11	Muffé Lake	391,295	5,054,715	2078			x			x	x

3.3. Laboratory Analyses

Chemical analyses were carried out at the hydrochemistry laboratory of the Earth Sciences Department of the University of Torino, according to standard methods [55–59]. The percentage error was calculated as:

$$[(\Sigma\text{cations} - \Sigma\text{anions})/(\Sigma\text{cations} + \Sigma\text{anions})] \times 100.$$

The pH measurements were taken using a Hanna Instrument H2211 pH/ORP meter (584 Park E Dr, Woonsocket, RI 02895, USA), calibrated with pH standards of 4.00, 7.00, and 10.00; electrolytic conductivity was measured using a Mettler Toledo Five Easy (1900 Polaris Pkwy, Columbus, OH 43240, USA), previously calibrated with a standard solution of KCl at 1462 μm and 25 °C. Both instruments were equipped with automatic temperature compensation. Total alkalinity (HCO_3^- and CO_3^{2-}) was determined by the acid-base titration method using a Metrohm 665 Dosimat (Lonenstrasse 9100 Herisau Switzerland) with 0.1 N HCl as the titration solution and a 100 mL sample. Methyl orange was used as a colour indicator. Anions and cations were determined by ion chromatography, in particular, chemical suppression ion chromatography for anions. Metrohm IC883 and Metrohm 863 systems equipped with Metrosep A-Supp4 250 and Metrosep C4 250 separation columns for anions and cations, respectively, were used.

Isotopic analyses were carried out at the Department of Land, Environment, Agriculture, and Forestry of the University of Padova. The off-axis integrated cavity output spectroscopy method was applied for these analyses, using a DLT-100 analyser (ABB-Los Gatos Research Inc, San Jose, CA, USA). The isotopic ratios of $^2\text{H}/^1\text{H}$ and $^{18}\text{O}/^{16}\text{O}$ were expressed as δ notation ($\delta = (\text{R}_{\text{sample}}/\text{R}_{\text{standard}} - 1) \times 1000$) with respect to the Vienna Standard Mean Ocean Water (V-SMOW) international standard. Three bracketing standards were systematically run-in analytical sessions. These standards, obtained from the Los Gatos Research Company, were calibrated according to International Atomic Energy Agency (IAEA) international standards. Analytical precision and accuracy, based on replicate analyses of standards, were better than 0.3‰ and 1.0‰ for $\delta^{18}\text{O}$ and $\delta^2\text{H}$, respectively [40]. The analytical procedure for stable water analyses is described in [60].

3.4. Chemical and Isotopic Data Interpretation

The chemical data were used in the Piper diagram to determine the facies of the waters sampled in the study area. On the other hand, the isotopic data were plotted on a diagram $\delta^2\text{H}$ vs. $\delta^{18}\text{O}$ and compared with the global ($\delta^2\text{H} = 8 \delta^{18}\text{O} + 10$) and local meteoric line ($\delta^2\text{H} = 8.04 \delta^{18}\text{O} + 11.47$) for northern Italy determined by [61]. Moreover, to highlight the relation between isotopes data and altitude, the $\delta^{18}\text{O}$ concentrations of 6 rainwater samples were plotted with the samples' altitudes. Isotopic values of the Perrot Spring were then plotted on the same diagram, to obtain the average aquifer recharge altitude.

4. Results

4.1. Climatic Setting of the Study Area

The analyses of average annual and monthly temperature for the period 2003–2022 highlighted a quite homogeneous situation over time (Figure 5). More specifically, average annual temperature ranges between 6.96 and 9.33 °C in the Chevrère Station. Average monthly temperatures show an exponential increase from January to July and then decrease until December, with a minimum average of 0.45 °C for January and a maximum average of 17.60 °C for July. The decrease (August–December) follows a sort of linear function.

Cumulative rainfall at the Chevrère Station for the period 2003–2022 (Figure 5) shows an annual average value of 863.61 mm/year, with a minimum value of 419 mm/year in 2022, and a maximum value of 1327 mm/year in 2018. The graphic evidence two predominantly rainy months on average, May, and November, with values of 115 mm and 112 mm, respectively (Figure 6).

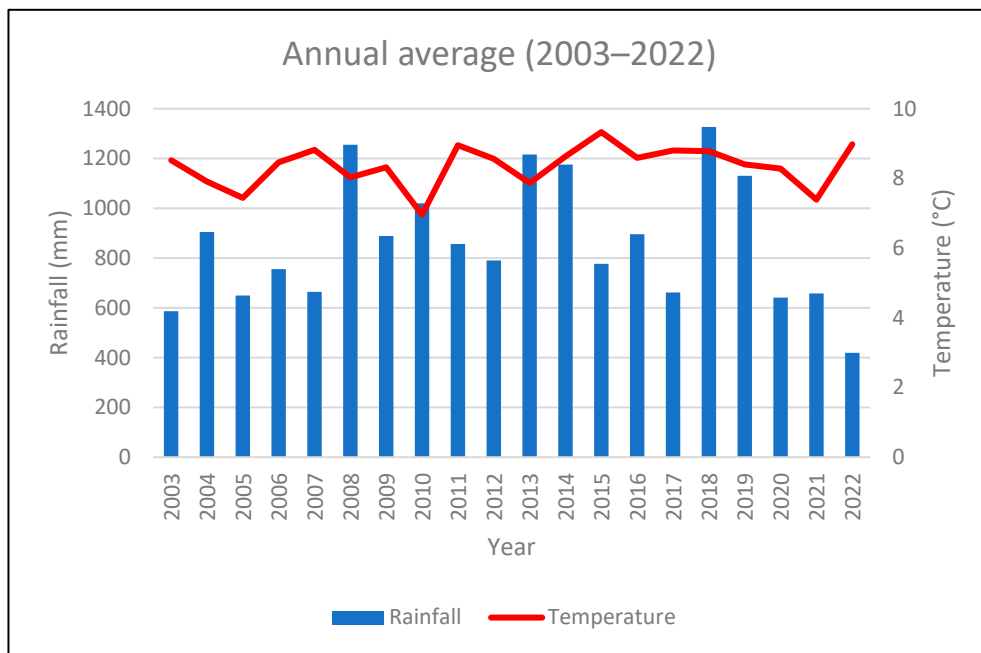


Figure 5. Average annual temperatures and rainfall for the period 2003–2022 at the Chevrère Station.

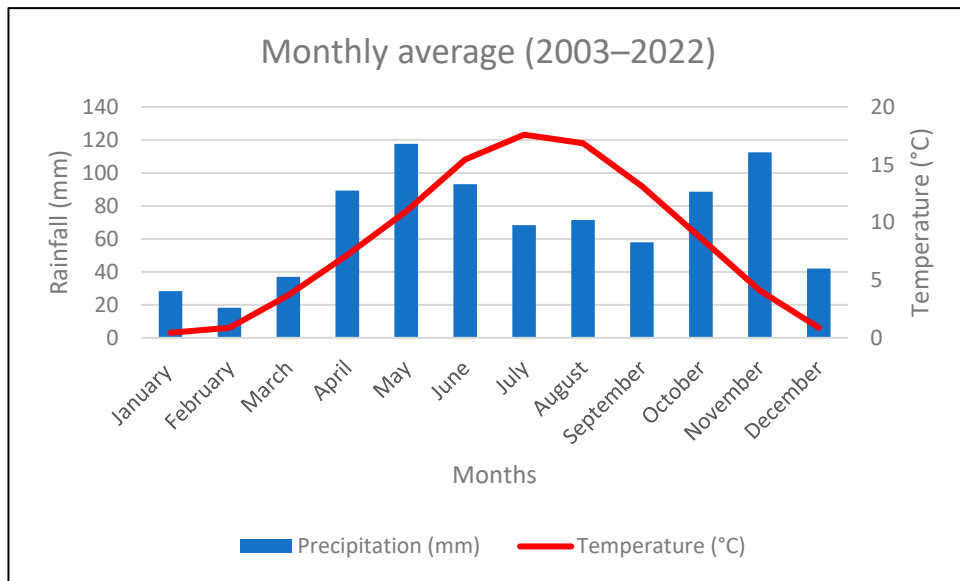


Figure 6. Average monthly temperature and rainfall for the period 2003–2022 at the Chevrère Station.

Monthly rainfall at the Chevrère Station from 2003 to 2022 is shown in Figure 6.

The thickness of the snow cover in the study area varies as a function of altitude, with the greatest thicknesses at the highest altitudes, ranging from 50–120 cm in 2021–2022 [62]. At the snow station closest to the study area (Champorcher station), the presence of snow on the ground was registered between November and May, with the maximum height in March [57]. The maximum average snow height in the period 1996–2019 reached 100 cm; the maximum snow height (250 cm) was measured in March 1996. In 2021–2022 the snow height remained below 50 cm. Considering that the study area is at a higher altitude than the Champorcher Station, it is likely that the snow height would have reached higher values in the period 2021–2022. The decrease in the snow cover between March and May indicates the prevalence of snow melt during this period (Figure 7).

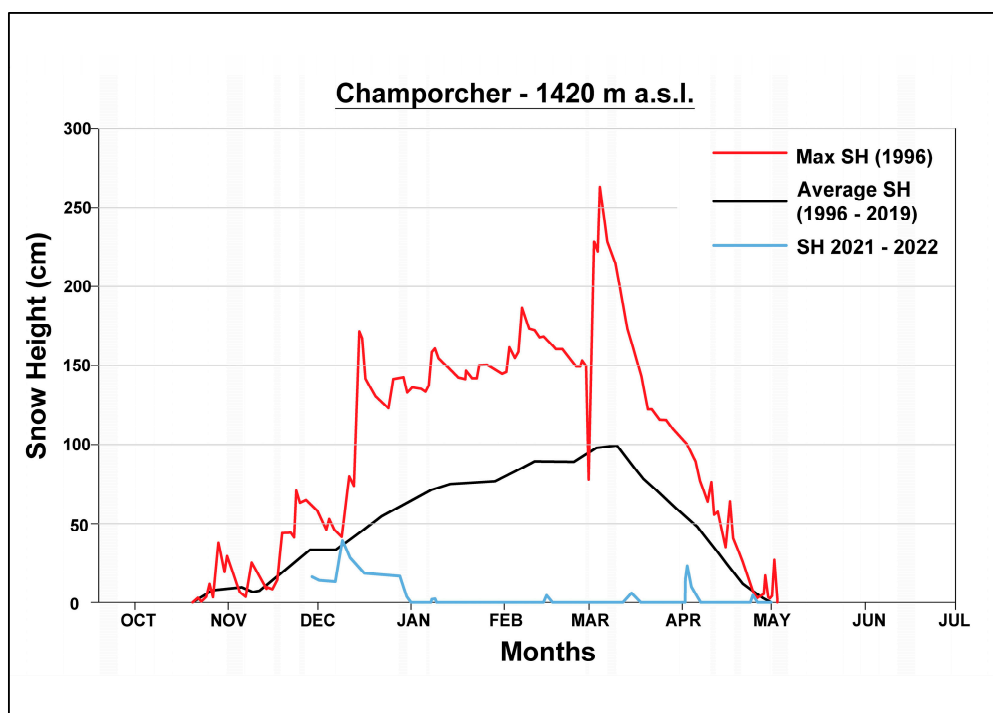


Figure 7. Snow height (SH) at Champorcher Station (modified from [62]).

4.2. Chemical Analysis

The results of the chemical and physico-chemical analyses conducted on water samples are reported in Table 3 (Figure 8). The calculated percentage error is generally less than 5%.

Table 3. Results of chemical and physico-chemical analyses of water.

ID	EC	pH	T	Na ⁺	K ⁺	Ca ²⁺	Mg ²⁺	Li ⁺	NH ₄ ⁺	Cl ⁻	NO ₂ ⁻	F ⁻	Br ⁻	HCO ₃ ⁻	SO ₄ ²⁻	NO ₃ ⁻	Error
S_1 (6 May 2021) Perrot Spring	81	8.20	4.8	N/A	N/A	10.33	4.30	N/A	N/A	1.50	N/A	N/A	N/A	51.90	2.10	2.80	N/A
S_1 (7 February 2022) Perrot Spring	88	9.40	5.0	N/A	N/A	3.70	9.90	N/A	N/A	0.55	N/A	N/A	N/A	57.83	2.10	2.50	N/A
S_1 (8 July 2022) Perrot Spring	87	8.89	6.5	0.34	0.39	4.82	11.21	0.05	0.05	0.25	<0.005	<0.010	<0.010	61.49	1.85	2.65	4.37
R_1 (8 July 2022) Chalamy Stream	29	7.64	10.7	0.18	0.08	3.18	3.13	<0.010	0.06	0.06	<0.005	<0.010	<0.010	20.98	2.82	0.40	1.8
R_2 (8 July 2022) Chalamy Stream	35	7.73	15.0	0.18	0.13	5.36	2.24	<0.010	0.08	0.15	<0.005	<0.010	<0.010	29.28	0.10	0.03	1.97
L_1 (8 July 2022) Leser Lake	118	9.26	18.3	0.22	0.28	3.04	17.35	<0.010	0.43	0.26	<0.005	<0.010	<0.010	82.96	4.19	1.66	4.57
L_2 (8 July 2022) Vallette Lake	68	8.81	22.1	0.24	0.15	6.97	5.78	<0.010	0.25	0.18	<0.005	<0.010	<0.010	26.84	19.36	0.07	0.25
L_3 (8 July 2022) Bianco Lake	67	8.93	17.3	0.32	0.53	7.23	4.10	<0.010	0.11	0.37	<0.005	0.15	<0.010	25.62	15.50	0.86	2.89
L_4 (8 July 2022) Nero Lake	65	7.89	13.5	0.25	0.26	8.55	4.85	<0.010	0.08	0.14	<0.005	<0.010	<0.010	27.82	17.19	1.13	0.7
L_5 (8 July 2022) Gran Lake	31	7.85	15.1	0.35	0.62	9.20	3.02	<0.010	0.09	0.12	<0.005	0.03	<0.010	20.25	22.30	0.37	4.09
L_6 (8 July 2022) Leita Lake	31	8.04	16.0	0.34	0.30	6.52	1.14	<0.010	0.13	0.13	<0.005	<0.010	<0.010	20.01	4.13	0.05	3.8
L_8 (8 July 2022) Leita Superiore Lake	74	7.73	15.5	3.50	0.40	6.60	0.40	<0.010	0.07	0.12	<0.005	0.03	<0.010	21.72	7.40	0.98	0.17
L_9 (8 July 2022) North of the Gran Lake	9	7.67	18.8	0.14	0.25	1.40	0.92	<0.010	0.18	0.04	<0.005	0.02	<0.010	9.76	0.88	0.03	3.40
L_10 (8 July 2022) Cornuto Lake	58	8.19	19.5	0.60	1.10	12.00	2.80	<0.010	0.11	0.36	<0.005	0.03	<0.010	36.60	13.39	0.91	0.89
L_11 (8 July 2022) Muffé Lake	176	8.79	18.2	0.26	0.21	7.22	<0.010	<0.010	0.12	0.25	<0.005	<0.010	<0.010	12.93	6.54	1.28	0.14

Note: ID: monitoring point; EC: $\mu\text{S}/\text{cm}$; T: $^{\circ}\text{C}$; (Na⁺, K⁺, Ca²⁺, Mg²⁺, Li⁺, NH₄⁺, Cl⁻, NO₂⁻, F⁻, Br⁻, HCO₃⁻, SO₄²⁻, NO₃⁻: mg/L); error: %; N/A: not analyzed.

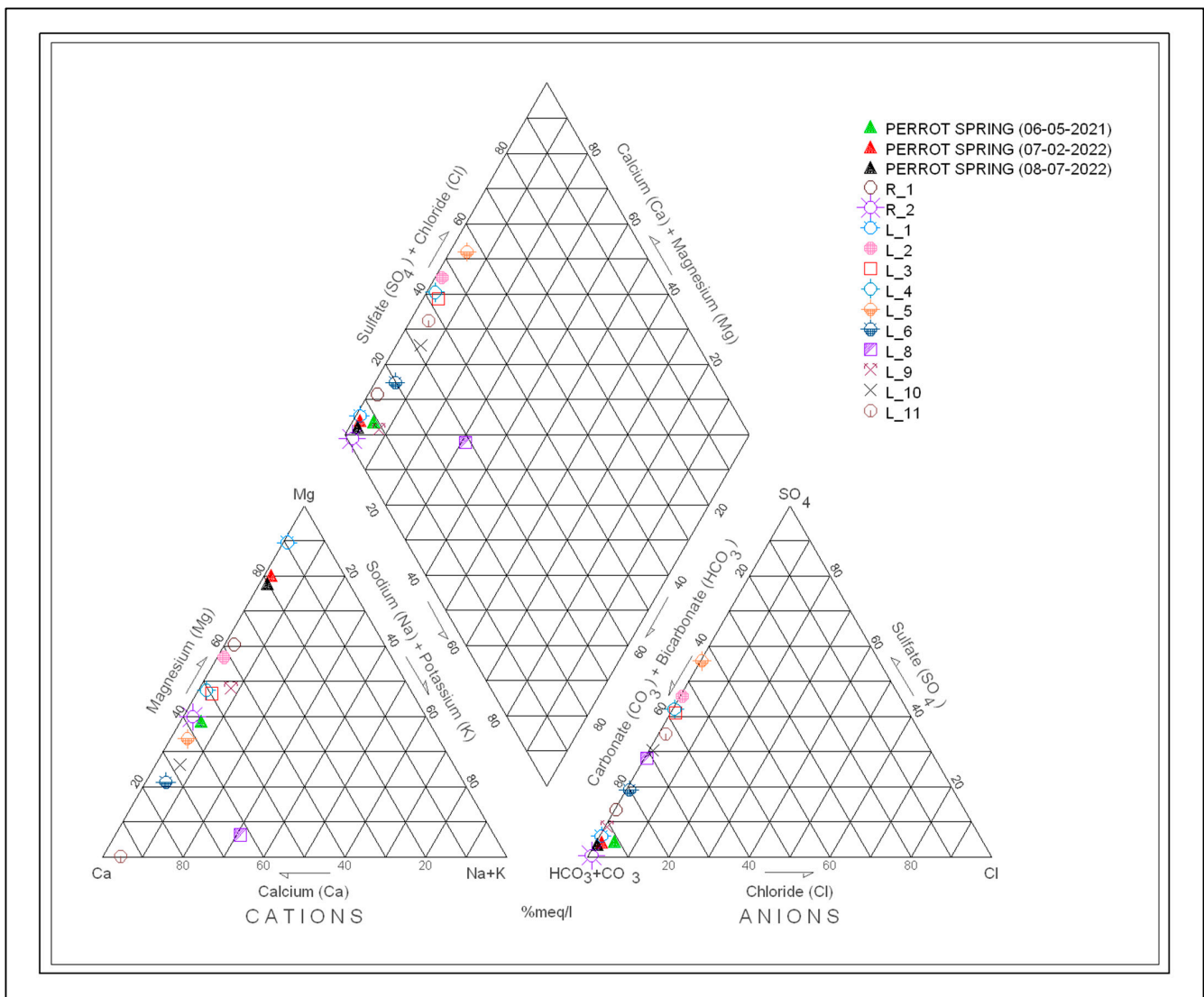


Figure 8. Piper diagram of the samples taken in various sites in July 2022 and in the Perrot Spring in February 2022 and May 2021. (R = stream; L = lake).

The EC varies from 9 $\mu\text{S}/\text{cm}$ to 176 $\mu\text{S}/\text{cm}$. The lowest EC value was found north of Gran Lake (L_9) and the maximum at Muffè Lake (L_11). The waters of the Perrot Spring (S_1) have an average value of 85 $\mu\text{S}/\text{cm}$. The values of EC increase with decreasing altitude; thus, EC generally increases moving from Leita Lake, Gran Lake, Cornuto Lake, Nero Lake, Bianco Lake, Vallette Lake, Leser Lake, to the Perrot Spring. The pH varies between 7.64 (R_1) and 9.40 (S_1), indicating a slightly alkaline character. The highest values are concentrated in the Chalamy Stream and in the Perrot Spring, with the pH decreasing with altitude. The Perrot Spring has an average value of 8.83. The water temperature is quite constant during the year, ranging from 4.8 to 6.5 $^{\circ}\text{C}$ (respectively, May and July). The average spring discharge ranges between 8 L/s (in October and April) and 45 L/s (in June and December). The increase in the discharge is connected to the spring thaw and autumn rainfall infiltration. The water of the Perrot Spring has the lowest temperatures and can be classified as cold according to the Mouren classification [63]. The warmest waters were measured in the lakes. The concentration of the main ions in the lakes and streams is usually very low. Almost all the sampled waters (the Perrot Spring and surface waters) belong to the calcium–magnesium bicarbonate facies (Figure 8). This hydrochemical facies is typical of surface cold and relatively recent groundwater. Samples L_2, L_5 and L_7 have a calcium–chloride-type nature.

4.3. Isotopic Analyses

Table 4 shows the results of the isotopic analyses carried out on surface water, ground-water, and rainwater for the 2021 and 2022 sampling campaigns. Regarding precipitation, it can be observed for each campaign that the most negative data relate to samples taken at higher elevations, while the least negative data relate to samples taken at lower elevations. The hydrogeological literature suggests that the most negative absolute data refer to the autumn and winter months [64]. The Perrot Spring (S_1) shows an almost equal value in the two sampling campaigns of May 2021 and July 2022.

Table 4. Results of isotopic analyses (2021–2022).

Monitoring Point ID	Year	2021				2022					
		Day	1 May		10 July		10 November		8 July		20 September
	Elevation	$\delta^2\text{H}$	$\delta^{18}\text{O}$	$\delta^2\text{H}$	$\delta^{18}\text{O}$	$\delta^2\text{H}$	$\delta^{18}\text{O}$	$\delta^2\text{H}$	$\delta^{18}\text{O}$	$\delta^2\text{H}$	$\delta^{18}\text{O}$
C_1 (Park office)	414	−26.4	−4.64			−72.2	−10.61	−40.3	−7.10	−30.1	−6.34
C_2 (Park Location 2)	965	−34.1	−5.72			−85.7	−12.35	−40.6	−7.54	−39.8	−7.76
C_3 (Park Location 3)	1269	−40.8	−6.57			−86.0	−12.41	−45.4	−8.22	−36.7	−7.14
C_4 (near Perrot Spring)	1561					−92.8	−13.24	−71.3	−11.13	−41.6	−7.53
C_5 (near Bianco Lake)	2160							−74.8	−11.19	−48.7	−8.65
C_6 (near Gran Lake)	2503									−52.5	−9.33
S_1 (Perrot Spring)	1300	−71.8	−10.49					−73.4	−11.06		
R_1 (Chalamy Stream)	2295							−96.0	−13.41		
R_2 (Chalamy Stream)	2532							−76.1	−11.42		
L_1 (Leser Lake)	2017							−68.7	−10.71		
L_2 (Vallette Lake)	2182							−61.8	−9.81		
L_3 (Bianco Lake)	2159			−74.7	−10.81			−58.5	−9.78		
L_4 (Nero Lake)	2169			−75.0	−11.08			−66.7	−10.65		
L_5 (Gran Lake)	2494			−79.7	−11.46			−71.6	−11.16		
L_6 (Leita Lake)	2532							−71.8	−11.27		
L_8 (Leita Superiore Lake)	2563							−73.7	−11.16		
L_9 (North of the Gran Lake)	2527							−78.1	−11.49		
L_10 (Cornuto Lake)	2173			−73.5	−10.89			−77.1	−11.52		
L_11 (Muffé Lake)	2078			−73.3	−10.88			−72.6	−11.13		

Note: (C = rain; S = Perrot Spring; R = stream; L = lake).

The plot of $\delta^2\text{H}$ vs. $\delta^{18}\text{O}$ considers precipitation (Figure 9), surface water, and ground-water (Figure 9). Rainfall isotope values are highly variable (with $\delta^2\text{H}$ from -92.76‰ to -26.37‰ ; and $\delta^{18}\text{O}$ from -13.24‰ to -4.64‰). Groundwater samples from the Perrot Spring have very similar values (with $\delta^2\text{H}$ from -73.38‰ to -71.83‰ ; and $\delta^{18}\text{O}$ from -11.06‰ to -10.49‰). Surface water has a slightly wider distribution of isotopic values than groundwater (with $\delta^2\text{H}$ from -96.01‰ to -58.54‰ ; and $\delta^{18}\text{O}$ from -13.41‰ to -9.78‰).

$\delta^{18}\text{O}$ data of rainfall (sampling campaign of May and November 2021 and July and September 2022) were averaged and then plotted against the altitude of sampling (Figure 10). Finally, they were compared with the $\delta^{18}\text{O}$ of the Perrot Spring (May 2021 and July 2022), in order to evaluate an average recharge altitude for the spring (Figure 10).

The average recharge elevation of the Perrot Spring was estimated to be around 1990–2210 m (average 2100 m a.s.l.).

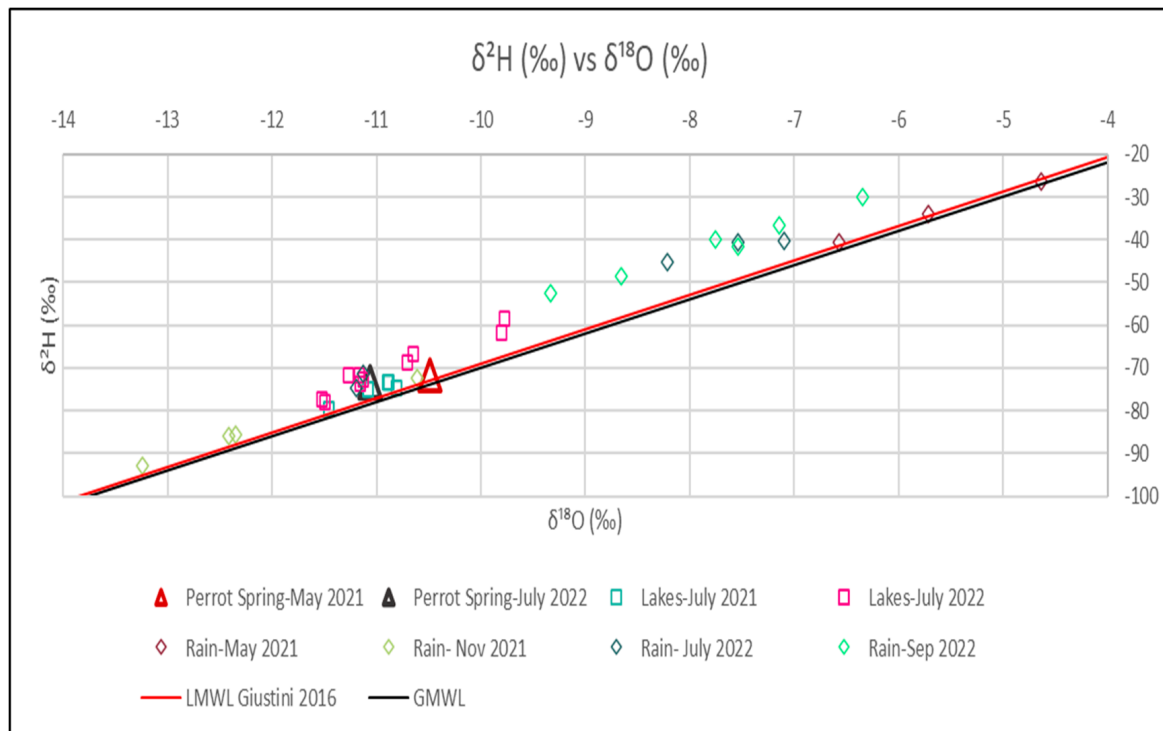


Figure 9. Isotopic composition of water samples in the study area. Global and local meteoric line for northern Italy (GMWL and LMWL) are also reported for the comparison [61].

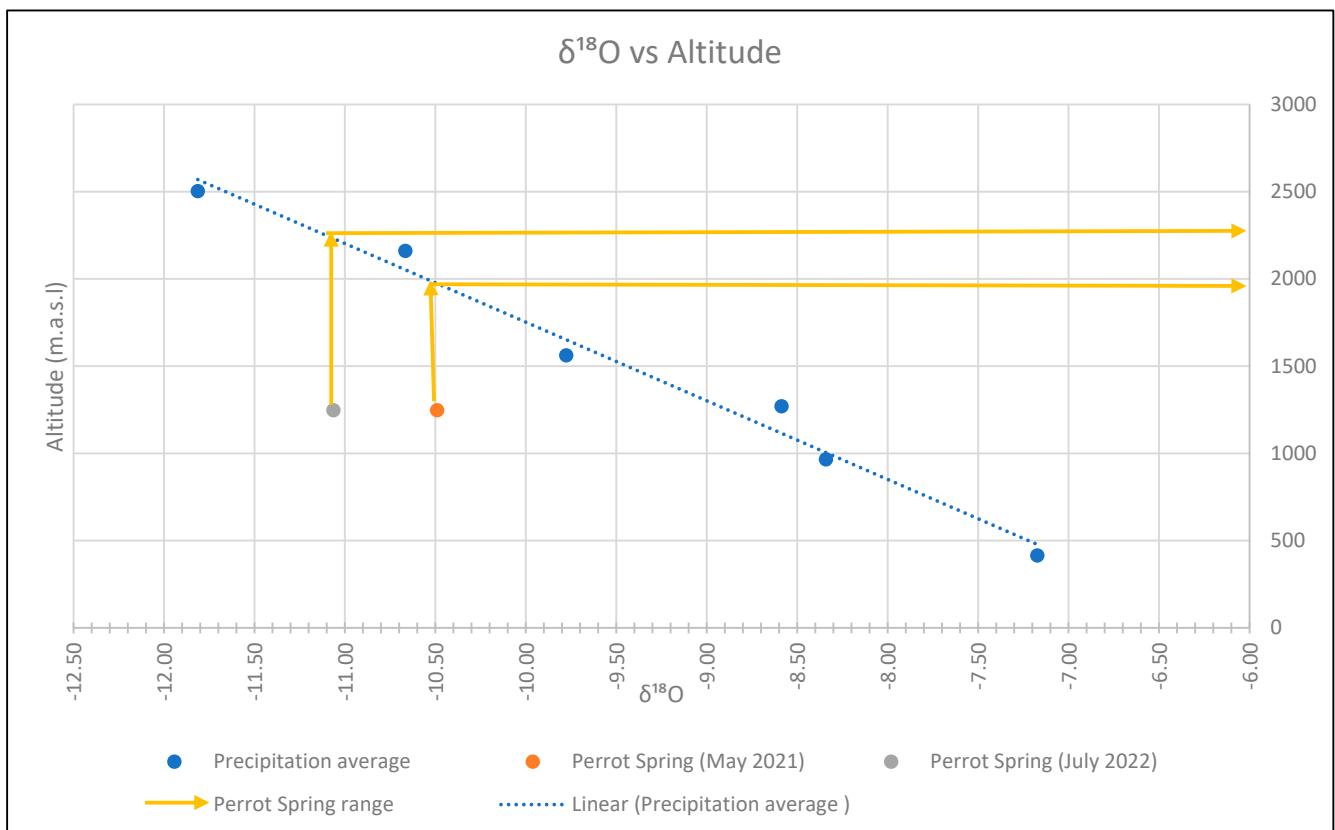


Figure 10. Correlation graph between the altitude of the sampling points and the value of $\delta^{18}\text{O}$.

5. Discussions

The EC of the samples shows rather low values, both in the groundwater and in the surface water, with the exception of the sample L_11 (Muffè Lake) which is located outside the study area (176 $\mu\text{S}/\text{cm}$). The pH has alkaline values both in the lakes and in the spring, up to 9.4.

The highest value of HCO_3^- (82.96 mg/L) was recorded in July 2022 in sample L_1 (Leser Lake). The bicarbonate concentration in the Perrot Spring varies between 51 and 61 mg/L in all three sampling campaigns, probably related to the presence of dissolved CO_2 in the rainwater that infiltrates the rocks of the area, the calcite veins, and the cementation of the Quaternary deposits. In addition, the contribution of carbon dioxide could be hypothesised from the large amount of organic matter present in the lake and marsh deposits close to the spring. The Perrot Spring shows intermediate values between the Lake Leser and the other lakes and streams samples, remaining in the range of 20 to 30 mg/L, with the exception of Gran Lake, which has a low concentration of 9.76 mg/L.

Nitrate concentrations are very low in the lakes and in the spring, below and above 3 mg/L, respectively. This indicates that there is almost no input of pollutants from agriculture, livestock, or infrastructure in the area. Furthermore, the presence of NH_4^+ in the lakes indicates the degradation of organic matter, suggesting an anoxic environment with probable denitrification processes. The chloride concentration shows a similar value (0.03–1.50 mg/L).

The Ca^{2+} and Mg^{2+} ions show concentrations ranging from 2 to 12 mg/L in streams, lakes, and springs. In the Perrot Spring, Ca^{2+} concentrations range from 3.7 mg/L to 10.3 mg/L, while Mg^{2+} concentrations range from 4.3 mg/L to 11.21 mg/L. Ca^{2+} can be essentially attributed to rich diopside rock and calcite veins. The Mg^{2+} can be attributed to the circulation of water, essentially within the serpentinite.

The Na^+ and K^+ ions are found in low concentrations (below 4 and 1.5 mg/L, respectively), probably due to the fact that the water circulates through rocks without K-feldspar, potassic phyllosilicates, and albite.

SO_4^{2-} shows a very low concentration in the spring (maximum value 2.1 mg/L) and higher concentrations in the lakes (maximum value 22.3 mg/L). These values and differences could be attributed to probable denitrification processes between the lakes and the spring.

From the graph of Figure 9, the isotopic composition of the lakes, rainfall, and the Perrot Spring appears to have a linear relationship. The groundwater flowing from the Perrot Spring shows values close to the average annual groundwater isotopic composition. Indeed, the isotopic composition of the groundwater flowing towards the Perrot Spring is a mixture of two water inputs: rainfall and contribution from the upper stretch of the Chalamy Stream also draining the lake area. According to the plotted data, the rainfall in November 2021 and September 2022 shows an Atlantic origin, while the rainfall in May 2021 and July 2022 indicates the influence of air masses from the Mediterranean basin, as reported by various authors (for example, [65]); specifically, their formation depends on the temperature, with rainfall with more negative isotopic values forming at lower temperatures and vice versa [64].

However, stable isotopic of water values do not coincide perfectly with the local meteoric water line LMWL in northern Italy, reported by [61]. Some possible explanations are: (i) LMWL is referred to a large area (the entire north Italy, with very low values in NW Italian Alps) while these analyses are very localized; and (ii) climate variations that can affect the isotopic values of water. Changes in temperature, rainfall patterns, or atmospheric circulation patterns due to climate change can cause deviations from the local meteoric water line [19,40].

Nevertheless, further studies and analyses may be required to determine a more precise local meteoric line in the study area and to compare it with the LMWL reported by [61].

Analysing the isotopic correlation between the Perrot Spring and the rainfall, an average recharge altitude from about 1990 and 2210 m a.s.l. was identified (Figure 10). This value can identify a recharge basin with a significant areal extent (Figure 11).

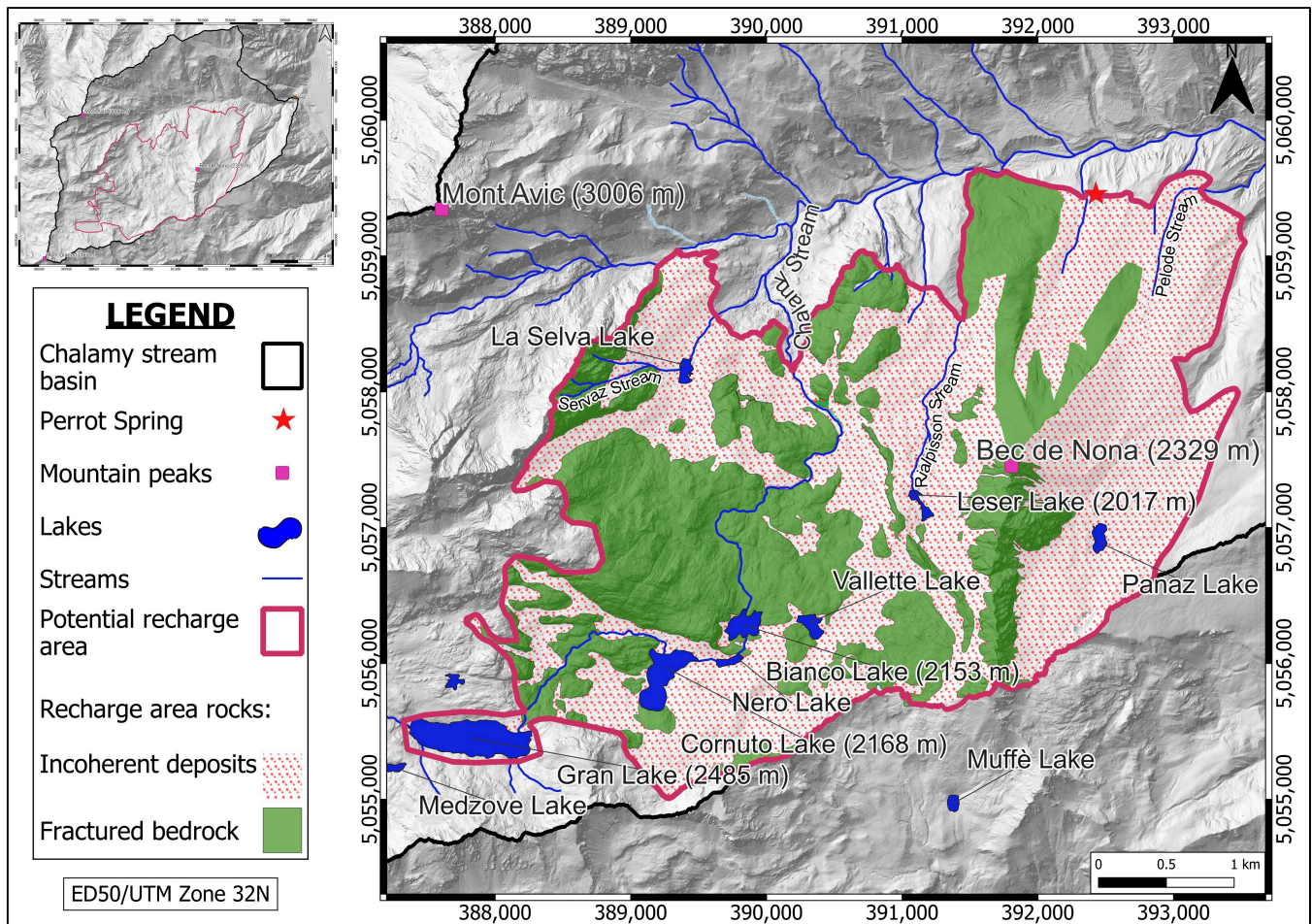


Figure 11. Potential recharge area.

The low ion concentrations are influenced by rainfall inputs and low water–rock interaction. In addition, the lithological uniformity of the study area does not lead to a relevant heterogeneity in the chemistry of the waters of the basin, and for this reason it is not possible to identify recharge areas based on ionic content alone.

Isotopic analyses confirm the mixing processes in relation to the average altitude of recharge, confirming that the spring is fed by both upland and lowland waters.

The results of the isotopic analyses conducted on the rainwater samples, the lake water, and the water from the Perrot Spring made it possible to identify an average feeding zone between 1990 and 2210 m above sea level. On the basis of the results of the above-mentioned laboratory tests, it was possible to identify a feeding zone of the Perrot Spring at an altitude range between 1710 and 2490 m a.s.l., which included a number of sectors that were probably capable of storing large quantities of water. In the present work, these sectors have been divided into two potential recharge areas, differentiated on the basis of the lithotype and the associated degree of permeability:

- fractured rocky bedrock with low to very low permeability, essentially represented by the serpentinite.
- very thick incoherent deposits of very high to high permeability, including ice-marginal, gravitational, and fluvial deposits that lie on incoherent deposits of low permeability, including subglacial and glaciolacustrine deposits.

The red line defines the possible feeding zone that is identified by a groundwater circuit within the discontinuities of the crystalline bedrock.

The underground flow, which follows the direction of the maximum hydraulic gradient, has a large main flow from SW to NE. Specifically, there is a local contribution from the slopes of Bec de Nona towards the spring (south to north), following a preferential path through the incoherent deposits present. There is also a local contribution from the Chalamy Stream that also drains the lake area towards the spring, following a path determined by the local topography. It is thought that this latter subterranean outflow may be accommodated in the incoherent deposits present on the surface and in the discontinuities of the rocky bedrock, the latter constituting a deeper water circuit. In addition, in relation to the geological setting, it is not possible to exclude a minority contribution to recharge from the southern sector outside the study area, corresponding to the northern slope of the Champorcher Valley (Figure 11).

6. Conclusions

The Perrot Spring, located in the Aosta Valley, is situated in a geologically rather heterogeneous area. In addition, its topography, in a mountainous relief with an altitude ranging from 950 to 2570 m a.s.l., makes the study of this sector very complex, also considering the difficulties in reaching the sampling points.

Hydrochemical and isotopic methods were used to understand the dynamics of groundwater flow, the altitude of groundwater recharge and the evolution of groundwater hydrochemistry in the study area.

The groundwater of the Perrot Spring comes mainly from atmospheric precipitation, snowmelt from the surrounding mountains and a contribution from the upper reaches of the Chalamy stream.

Water–rock interaction and mixing processes control the chemistry and stable isotope composition of the Perrot Spring water. Low ion concentrations are influenced by rainfall inputs and scarce water–rock interaction.

Based on hydrochemistry, the water of the Perrot Spring dissolves mainly minerals from ophiolitic rocks and from glacial deposits. The low temperature and the weak yearly temperature variation in the Perrot Spring suggest a relatively high average recharge area, and a sufficiently deep flow circuit.

The recharge zone evaluated with stable isotopes of water is located between 1990 and 2210 m a.s.l., and the direction of flow is mainly controlled by the north-facing slope of the Chalamy Basin.

Future research would focus not only on the quality of surface and groundwater in the study area, but also on their availability. Both aspects are of utmost importance when dealing with mountainous water resources and are strategically important for the maintenance of water supply for human consumption and the preservation of ecosystems, also dealing with climate change and human growth.

Author Contributions: Conceptualization, L.M.S.-Q., M.L., D.A.D.L., M.G.F. and M.G.; methodology, M.L. and D.A.D.L.; software, L.M.S.-Q., G.V. and D.C.; validation, M.L. and D.A.D.L.; formal analysis, E.D. and C.M.; investigation, L.M.S.-Q., G.V. and D.C.; resources, M.L. and D.A.D.L.; data curation, L.M.S.-Q., G.V. and D.C.; writing—original draft preparation, L.M.S.-Q., G.V. and D.C.; writing—review and editing, M.L., D.A.D.L., M.G.F. and M.G.; visualization, L.M.S.-Q., G.V., D.C., M.L., D.A.D.L., M.G. and M.G.; supervision, M.L., D.A.D.L., M.G.F. and M.G.; project administration, M.L., D.A.D.L., M.G.F. and M.G.; funding acquisition, D.A.D.L. and M.L. All authors have read and agreed to the published version of the manuscript.

Funding: This research received no external funding.

Data Availability Statement: I point out that all data are collected in the field by the authors and published here for the first time. I use public datasets.

Acknowledgments: The authors would like to thank the Mont Avic Natural Park Authority for the data provided and for their co-operation during the study.

Conflicts of Interest: The authors declare no conflict of interest.

References

1. The United Nations World Water Development. *Groundwater: Making the Invisible Visible*; The United Nations World Water Development: Paris, France, 2022.
2. Bowen, G.J.; Ehleringer, J.R.; Chesson, L.A.; Stange, E.; Cerling, T.E. Stable Isotope Ratios of Tap Water in the Contiguous United States. *Water Resour. Res.* **2007**, *43*, W03419. [[CrossRef](#)]
3. De Luca, D.A.; Masciocco, L.; Caviglia, C.; Destefanis, E.; Forno, M.G.; Fratianni, S.; Gattiglio, M.; Gianotti, F.; Lasagna, M.; Latagliata, V.; et al. Distribution, Discharge, Geological and Physical–Chemical Features of the Springs in the Turin Province (Piedmont, NW Italy). In *Engineering Geology for Society and Territory-Volume 3*; Springer International Publishing: Cham, Switzerland, 2015; pp. 253–256. [[CrossRef](#)]
4. Fiorillo, F.; Pagnozzi, M.; Stevanović, Z.; Ventafridda, G. Main hydrological features and recharge analysis of the Caposele Spring Catchment, Southern Italy. *Acta Carsologica* **2019**, *48*, 6738. [[CrossRef](#)]
5. Cusano, D.; Allocca, V.; Coda, S.; Lepore, D.; Vassallo, M.; De Vita, P. The Survey of Italian Springs by the National Hydrographic Service, a Forgotten Database. Structuring and Analysis of a Dataset of Campania Springs (Southern Italy). *Acque Sotter. Ital. J. Groundw.* **2022**, *11*, 31–41. [[CrossRef](#)]
6. Vigna, B.; Banzato, C. The Hydrogeology of High-Mountain Carbonate Areas: An Example of Some Alpine Systems in Southern Piedmont (Italy). *Environ. Earth Sci.* **2015**, *74*, 267–280. [[CrossRef](#)]
7. Howell, B.A.; Fryar, A.E.; Benaabidate, L.; Bouchaou, L.; Farhaoui, M. Variable Responses of Karst Springs to Recharge in the Middle Atlas Region of Morocco. *Hydrogeol. J.* **2019**, *27*, 1693–1710. [[CrossRef](#)]
8. Bastiancich, L.; Lasagna, M.; Mancini, S.; Falco, M.; De Luca, D.A. Temperature and discharge variations in natural mineral water springs due to climate variability: A case study in the Piedmont Alps (NW Italy). *Environ. Geochem. Health* **2022**, *44*, 1971–1994. [[CrossRef](#)]
9. Fensham, R.J.; Doyle, T.; Habermehl, M.A.; Laffineur, B.; Silcock, J.L. Hydrogeological assessment of Springs in the South-Central Great Artesian Basin of Australia. *Hydrogeol. J.* **2021**, *29*, 1501–1515. [[CrossRef](#)]
10. Galleani, L.; Vigna, B.; Banzato, C.; Russo, S.L. Validation of a Vulnerability Estimator for Spring Protection Areas: The VESPA Index. *J. Hydrol.* **2011**, *396*, 233–245. [[CrossRef](#)]
11. Stevens, L.E.; Schenk, E.R.; Springer, A.E. Springs Ecosystem Classification. *Ecol. Appl.* **2021**, *31*, 2218. [[CrossRef](#)] [[PubMed](#)]
12. Petitta, M.; Banzato, F.; Lorenzi, V.; Matani, E.; Sbarbati, C. Determining Recharge Distribution in Fractured Carbonate Aquifers in Central Italy Using Environmental Isotopes: Snowpack Cover as an Indicator for Future Availability of Groundwater Resources. *Hydrogeol. J.* **2022**, *30*, 1619–1636. [[CrossRef](#)]
13. Lasagna, M.; De Luca, D.A.; Clemente, P.; Dino, G.A.; Forno, M.G.; Gattiglio, M.; Gianotti, F. Study on the Water Supply of the Montellina Spring by the Renanchio Stream (Quincinetto, Turin). *Acque Sotter. Ital. J. Groundw.* **2013**, *2*, 75–85. [[CrossRef](#)]
14. De Luca, D.A.; Cerino Abidin, E.; Forno, M.G.; Gattiglio, M.; Gianotti, F.; Lasagna, M. The Montellina Spring as an Example of Water Circulation in an Alpine DSGSD Context (NW Italy). *Water* **2019**, *11*, 700. [[CrossRef](#)]
15. Yu, S.; Chae, G.; Oh, J.; Kim, S.-H.; Kim, D.-I.; Yun, S.-T. Hydrochemical and Isotopic Difference of Spring Water Depending on Flow Type in a Stratigraphically Complex Karst Area of South Korea. *Front. Earth Sci.* **2021**, *9*, 712865. [[CrossRef](#)]
16. Cocca, D.; Lasagna, M.; Marchina, C.; Brombin, V.; Santillan-Quiroga, L.M.; De Luca, D.A. Assessment of the Groundwater Recharge Processes of a Shallow and Deep Aquifer System (Maggiore Valley, Northwest Italy): A Hydrogeochemical and Isotopic Approach. *Hydrogeol. J.* **2023**, 1–22. [[CrossRef](#)]
17. Bian, J.; Sun, W.; Li, J.; Li, Y.; Ma, Y.; Li, Y. Hydrochemical Formation Mechanism of Mineral Springs in Changbai Mountain (China). *Environ. Earth Sci.* **2023**, *82*, 145. [[CrossRef](#)]
18. Barbata, A.; Ogée, J.; Peñuelas, J. Stable-Isotope Techniques to Investigate Sources of Plant Water. In *Advances in Plant Ecophysiology Techniques*; Springer International Publishing: Cham, Switzerland, 2018; pp. 439–456. [[CrossRef](#)]
19. Sprenger, M.; Weiler, M.; Volkmann, T.H. A Global Review on Isotopic and Hydrochemical Studies of the Unsaturated Zone. *Earth-Sci. Rev.* **2018**, *185*, 150–171.
20. Gat, J.R. Oxygen and Hydrogen Isotopes in the Hydrologic Cycle. *Annu. Rev. Earth Planet. Sci.* **1996**, *24*, 225–262. [[CrossRef](#)]
21. West, J.B.; Bowen, G.J.; Cerling, T.E.; Ehleringer, J.R. Stable Isotopes as One of Nature’s Ecological Recorders. *Trends Ecol. Evol.* **2006**, *21*, 408–414. [[CrossRef](#)]
22. Chen, K.; Tetzlaff, D.; Goldammer, T.; Freymueller, J.; Wu, S.; Andrew Smith, A.; Schmidt, A.; Liu, G.; Venohr, M.; Soulsby, C. Synoptic Water Isotope Surveys to Understand the Hydrology of Large Intensively Managed Catchments. *J. Hydrol.* **2023**, *623*, 129817. [[CrossRef](#)]
23. Windhorst, D.; Waltz, T.; Timbe, E.; Frede, H.-G.; Breuer, L. Impact of Elevation and Weather Patterns on the Isotopic Composition of Precipitation in a Tropical Montane Rainforest. *Hydrol. Earth Syst. Sci.* **2013**, *17*, 409–419. [[CrossRef](#)]
24. Novel, J.P.; Ravello, M.; Dray, M.; Pollicini, F.; Zuppi, G.M. Isotopic Contribution (^{18}O , ^2H , ^3H) in the Understanding of the Flow Pattern in Surface Water and Groundwater in the Aosta Valley (Italy). *Geogr. Fis. Din. Quat.* **1995**, *18*, 315–319.
25. Calligaris, C.; Mezga, K.; Slejko, F.; Urbanc, J.; Zini, L. Groundwater Characterization by Means of Conservative ($\delta^{18}\text{O}$ and $\delta^2\text{H}$) and non-conservative ($^{87}\text{Sr}/^{86}\text{Sr}$) Isotopic Values: The Classical Karst Region Aquifer Case (Italy–Slovenia). *Geosciences* **2018**, *8*, 321. [[CrossRef](#)]

26. Capecchiacci, F.; Tassi, F.; Vaselli, O.; Bicocchi, G.; Cabassi, J.; Giannini, L.; Nisi, B.; Chiocciara, G. A Combined Geochemical and Isotopic Study of the Fluids Discharged from the Montecatini Thermal System (NW Tuscany, Italy). *Appl. Geochem.* **2015**, *59*, 33–46. [[CrossRef](#)]
27. Frondini, F.; Zucchini, A.; Comodi, P. Water-Rock Interactions and Trace Elements Distribution in Dolomite Aquifers: The Sassolungo and Sella Systems (Northern Italy). *Geochem. J.* **2014**, *48*, 231–246. [[CrossRef](#)]
28. Edmunds, W.M.; Smedley, P.L. Residence time indicators in groundwater: The East Midlands Triassic sandstone aquifer. *Appl. Geochem.* **2000**, *15*, 737–752. [[CrossRef](#)]
29. Bouchaou, L.; Michelot, J.L.; Vengosh, A.; Hsissou, Y.; Qurtobi, M.; Gaye, C.B.; Bullen, T.D.; Zuppi, G.M. Application of Multiple Isotopic and Geochemical Tracers for Investigation of Recharge, Salinization, and Residence Time of Water in the Souss–Massa Aquifer, Southwest of Morocco. *J. Hydrol.* **2008**, *352*, 267–287. [[CrossRef](#)]
30. Joshi, S.K.; Rai, S.P.; Sinha, R.; Gupta, S.; Densmore, A.L.; Rawat, Y.S.; Shekhar, S. Tracing Groundwater Recharge Sources in the Northwestern Indian Alluvial Aquifer Using Water Isotopes ($\delta^{18}\text{O}$, $\delta^2\text{H}$ and ^3H). *J. Hydrol.* **2018**, *559*, 835–847. [[CrossRef](#)]
31. Terzer, S.; Wassenaar, L.I.; Araguás-Araguás, L.J.; Aggarwal, P.K. Global Isoscapes for $\delta^{18}\text{O}$ and $\delta^2\text{H}$ in Precipitation: Improved Using Regionalized Climatic Regression Models. *Hydrol. Earth Syst. Sci.* **2013**, *17*, 4713–4728. [[CrossRef](#)]
32. Gaj, M.; Beyer, M.; Koeniger, P.; Wanke, H.; Hamutoko, J.; Himmelsbach, T. In Situ Unsaturated Zone Water Stable Isotope ($\delta^2\text{H}$ and $\delta^{18}\text{O}$) Measurements in Semi-Arid Environments: A Soil Water Balance. *Hydrol. Earth Syst. Sci.* **2016**, *20*, 715–731. [[CrossRef](#)]
33. von Freyberg, J.; Studer, B.; Kirchner, J.W. A Lab in the Field: High-Frequency Analysis of Water Quality and Stable Isotopes in Stream Water and Precipitation. *Hydrol. Earth Syst. Sci.* **2017**, *21*, 1721–1739. [[CrossRef](#)]
34. Sánchez-Murillo, R.; Durán-Quesada, A.M.; Esquivel-Hernández, G.; Rojas-Cantillano, D.; Birkel, C.; Welsh, K.; Sánchez-Llull, M.; Alonso-Hernández, C.M.; Tetzlaff, D.; Soulsby, C.; et al. Deciphering Key Processes Controlling Rainfall Isotopic Variability during Extreme Tropical Cyclones. *Nat. Commun.* **2019**, *10*, 4321. [[CrossRef](#)] [[PubMed](#)]
35. Stichler, W.; Schotterer, U.; Fröhlich, K.; Ginot, P.; Kull, C.; Gäggeler, H.; Pouyaud, B. Influence of Sublimation on Stable Isotope Records Recovered from High-altitude Glaciers in the Tropical Andes. *J. Geophys. Res. Atmos.* **2001**, *106*, 22613–22620. [[CrossRef](#)]
36. Manciatì, C.; Taupin, J.D.; Patris, N.; Leduc, C.; Casiot, C. Diverging Water Ages Inferred from Hydrodynamics, Hydrochemical and Isotopic Tracers in a Tropical Andean Volcano-Sedimentary Confined Aquifer System. *Front. Water* **2021**, *3*, 597641. [[CrossRef](#)]
37. Yang, K.; Han, G.; Liu, M.; Li, X.; Liu, J.; Zhang, Q. Spatial and Seasonal Variation of O and H Isotopes in the Jiulong River, Southeast China. *Water* **2018**, *10*, 1677. [[CrossRef](#)]
38. Sun, Z.; Hu, C.; Wu, D.; Chen, G.; Lu, X.; Liu, X. Estimation of Evaporation Losses Based on Stable Isotopes of Stream Water in a Mountain Watershed. *Acta Geochim.* **2021**, *40*, 176–183. [[CrossRef](#)]
39. Darling, W.G.; Bath, A.H.; Talbot, J.C. The O and H Stable Isotopic Composition of Fresh Waters in the British Isles. 2. Surface Waters and Groundwater. *Hydrol. Earth Syst. Sci.* **2003**, *7*, 183–195. [[CrossRef](#)]
40. Marchina, C.; Zuecco, G.; Chiogna, G.; Bianchini, G.; Carturan, L.; Comiti, F.; Engel, M.; Natali, C.; Borga, M.; Penna, D. Alternative Methods to Determine the $\delta^2\text{H}$ - $\delta^{18}\text{O}$ Relationship: An Application to Different Water Types. *J. Hydrol.* **2020**, *587*, 124951. [[CrossRef](#)]
41. Bearth, P. *Die Ophiolithe Der Zone Von Zermatt-Saas Fee*; Kümmerly & Frey: Bern, Switzerland, 1967; 130P.
42. Bucher, K. Blueschists, Eclogites, and Decompression Assemblages of the Zermatt-Saas Ophiolite: High-Pressure Metamorphism of Subducted Tethys Lithosphere. *Am. Mineral.* **2005**, *90*, 821–835. [[CrossRef](#)]
43. Piazz, G.V.D.; Ernst, W.G. Areal Geology and Petrology of Eclogites and Associated Metabasites of the Piemonte Ophiolite Nappe, Breuil–St. Jacques Area, Italian Western Alps. *Tectonophysics* **1978**, *51*, 99–126. [[CrossRef](#)]
44. Dal Piazz, G.; Cortiana, G.; Del Moro, A.; Martin, S.; Pennacchioni, G.; Tartarotti, P. Tertiary Age and Paleostuctural Inferences of the Eclogitic Imprint in the Austroalpine Outliers and Zermatt–Saas Ophiolite, Western Alps. *Int. J. Earth Sci.* **2001**, *90*, 668–684. [[CrossRef](#)]
45. Reinecke, T. Prograde High- to Ultrahigh-Pressure Metamorphism and Exhumation of Oceanic Sediments at Lago Di Cignana, Zermatt-Saas Zone, Western Alps. *Lithos* **1998**, *42*, 147–189. [[CrossRef](#)]
46. Fontana, E.; Panseri, M.; Tartarotti, P. Oceanic Relict Textures in the Mount Avic Serpentinites, Western Alps. *Ophioliti* **2008**, *33*, 105–118.
47. Zanoni, D.; Rebay, G.; Bernardoni, J.; Spalla, M.I. Using Multiscale Structural Analysis to Infer High-/Ultrahigh-Pressure Assemblages in Subducted Rodingites of the Zermatt-Saas Zone at Valtournanche, Italy. *J. Virtual Explor.* **2012**, *41*, 290. [[CrossRef](#)]
48. Martin, S.; Tartarotti, P. Polyphase HP Metamorphism in the Ophiolitic Glaucophanites of the Lower St. Marcel Valley (Aosta, Italy). *Ophioliti* **1989**, *14*, 135–156.
49. Tartarotti, P.; Benciolini, L.; Monopoli, B. Breccie Serpentiniche Nel Massiccio Ultrabascico Del Monte Avic (Falda Ophiolitica Piemontese): Possibili Evidenze Di Erosione Sottomarina. *Atti Tic Sc. Terra* **1998**, *7*, 73–86.
50. Fontana, E.; Tartarotti, P.; Panseri, M.; Buscemi, S. Geological Map of the Mount Avic Massif (Western Alps Ophiolites). *J. Maps* **2015**, *11*, 126–135. [[CrossRef](#)]
51. Martin, S.; Kienast, J.R. The HP-LT Manganiferous Quartzites of Praborna. Piemonte Ophiolite Nappe. Italian Western Alps. *Schweiz. Mineral. Und Petrogr. Mitteilungen* **1987**, *67*, 339–360.
52. Forno, M.G.; Gattiglio, M.; Ghignone, S.; De Luca, D.A.; Santillan Quiroga, L.M. Geological Significance of the Perrot Spring in Mont Avic Natural Park (NW Alps). *Water* **2023**, *15*, 3042. [[CrossRef](#)]

53. Dal Piaz, G.V.; Gianotti, F.; Monopoli, B.; Pennacchioni, G.; Tartarotti, P.; Schiavo, A. Note Illustrative Della Carta Geologica d'Italia Alla Scala 1:50.000. Foglio 091 "Chatillon". Regione Autonoma Valle D'Aosta, Italy, 2010.
54. Centro Funzionale Regione Autonoma Vall'Aosta. *Dati Osservati del Centro Funzionale RAVDA*. Available online: https://presidi2.regione.vda.it/str_dataview_download (accessed on 7 July 2023).
55. ISO 7888:1985; Water Quality Determination of Electrical Conductivity. International Organization for Standardization: Geneva, Switzerland, 2023. Available online: <https://www.iso.org/standard/14838.html> (accessed on 26 May 2023).
56. ISO 10523:2008; Water Quality Determination of PH. International Organization for Standardization: Geneva, Switzerland, 2023. Available online: <https://www.iso.org/standard/51994.html> (accessed on 26 May 2023).
57. U.S. EPA Method 300.1, Determination of Inorganic Anions in Drinking Water by Ion Chromatography. U.S. Cincinnati; 1997. Available online: <https://www.epa.gov/esam/epa-method-3001-revision-10-determination-inorganic-anions-drinking-water-ion-chromatography> (accessed on 26 May 2023).
58. ISO 14911:1998; Water Quality Determination of Dissolved Li+, Na+, NH4+, K+, Mn2+, Ca2+, Mg2+, Sr2+ and Ba2+ Using Ion Chromatography Method for Water and Wastewater. International Organization for Standardization: Geneva, Switzerland, 2019. Available online: <https://www.iso.org/standard/25591.html> (accessed on 26 May 2023).
59. ISO 9963-1:1994; Water Quality Determination of Alkalinity Part 1: Determination of Total and Composite Alkalinity. International Organization for Standardization: Geneva, Switzerland, 2021. Available online: <https://www.iso.org/standard/17868.html> (accessed on 26 May 2023).
60. Zuecco, G.; Marchina, C.; Gelmini, Y.; Amin, A.; van Meerveld, H.J.; Penna, D.; Borga, M. Ressi Experimental Catchment: Ecohydrological Research in the Italian pre-Alps. *Hydrol. Process.* **2021**, *35*, 3. [[CrossRef](#)]
61. Giustini, F.; Brilli, M.; Patera, A. Mapping Oxygen Stable Isotopes of Precipitation in Italy. *J. Hydrol. Reg. Stud.* **2016**, *8*, 162–181. [[CrossRef](#)]
62. AINEVA. Analisi Meteo-Climatologiche e Nivo-Valangologiche su Alpi e Appennini 2021-22. Neve e Valanghe-Aineva. Available online: <https://aineva.it/pubblicazioni/resoconto-inverno-2021-22/> (accessed on 25 September 2023).
63. Celico, P. *Prospezioni Idrogeologiche*; Liguori Editore: Napoli, Italy, 1986; Volume 2, Available online: <https://catalogo-unito.sebina.it/SebinaOpac/resource/prospezioni-idrogeologiche/UTO01172659?tabDoc=tabcontiene> (accessed on 25 September 2023).
64. Grappein, B.; Lasagna, M.; Capodaglio, P.; Caselle, C.; De Luca, D.A. Hydrochemical and Isotopic Applications in the Western Aosta Valley (Italy) for Sustainable Groundwater Management. *Sustainability* **2021**, *13*, 487. [[CrossRef](#)]
65. Scandellari, F. Gli Isotopi Stabili Nell'acqua Fra Suolo, Pianta e Atmosfera. *Italus Hortus* **2018**, *24*, 51–67. [[CrossRef](#)]

Disclaimer/Publisher's Note: The statements, opinions and data contained in all publications are solely those of the individual author(s) and contributor(s) and not of MDPI and/or the editor(s). MDPI and/or the editor(s) disclaim responsibility for any injury to people or property resulting from any ideas, methods, instructions or products referred to in the content.